FREE VORTICITY FIELD-BOUNDARY LAYER CONVERSIONS:

EFFECT OF BOUNDARY CONFIGURATION AND SCALE

by

D. Rockwell, D. Sohn, and I. Gursul
Department of Mechanical Engineering and Mechanics
Lehigh University
Bethlehem, Pennsylvania 18015

PROGRESS REPORT ON NASA-LANGLEY GRANT "FREE VORTICITY FIELD-BOUNDARY
LAYER CONVERSIONS: EFFECTIVE BOUNDARY CONFIGURATION SCALE"

During the past six months substantial progress has been made on
further flow visualization of vortex-leading edge interaction, in conjunction
with characterization of the unsteady pressure field. The overall objective
of this investigation is to compare the detailed flow structure and induced
pressure with those previously obtained for a very thin leading-edge.

Figures 1 and 2 review previous findings for vortex-thin leading-edge
interaction. Figure 1 shows interaction of a single vortex with a sharp
leading-edge. It is evident that the distortion of the primary vortex and
the scale of the induced secondary vortex are strong functions of the
transverse location of the leading-edge with respect to the incident vortex.
As shown in Figure 2, a central feature of the secondary vortex formation
is migration of the fluid from the tip to the bottom surface of the tip of
the edge, driven by the interaction and distortion of the primary vortex
(not evident in this series of photos).

In the current investigation, we determine the range of scale of an
elliptical leading edge, relative to the incident primary vortex, for which
there are similar effects as shown in Figures 1 and 2 for the case of the
thin leading-edge. That is, we desire to determine the threshold value of
the thickness 2T of the 5:1 elliptical edge for which the mechanisms
characteristic of thin leading-edge interaction no longer occur. In all
cases, precisely the same values of incident vortex scale and concentration of
vorticity were employed as for the cases shown in Figures 1 and 2. The edge
scale was altered by machining 5:1 elliptical edges of various thicknesses.
The scale of the incident vortex was characterized in terms of mean shear
layer parameters; there is a direct relation between the thickness of the
shear layer and the scale of the fluctuating vorticity field associated with
the incident vortex. In essence, two parameters were considered: the
vorticity thickness of the incident shear layer, defined by $\Delta\omega = \Delta U/(dU/dy)_{max}$
where ΔU is the free stream velocity difference across the shear layer; and
momentum thickness θ_R of the incident shear layer defined using the traditional
definition of momentum thickness. Figure 3 shows the vortex-elliptical edge
interaction for the case where the total thickness of the edge is less than

the vorticity thickness of the incident shear layer, i.e. $2T/\Delta\omega = 0.7$.
It is evident that there is severing of the incident vortex and generation
of a secondary vortex in much the same fashion as the case of the thin
leading edge shown in Figures 1 and 2. On the other hand, if the thickness
of the leading edge is increased, by a factor of 6, corresponding to
$2T/\Delta\omega = 4.2$, then, as shown in Figure 4, there is no longer severing of
the incident vortical structure. Moreover, the secondary vortex is actually
formed downstream of, rather than at, the tip of the leading-edge. To gain
further insight into the delayed secondary vortex formation on a thick
leading-edge, the sequence of Figure 5 was taken with the hydrogen bubble
wire located at the tip of the leading-edge. Here, it is evident that
there is pronounced secondary vortex formation downstream of the tip
accompanied by continued development of the incident primary vortex, which
is evident in the bottom part of each of the photos.

An overview of the interaction mechanism for the range of thin to thick
leading-edges is given in Figure 6, which provides a time sequence of the
interaction process. The scale of the leading-edges and the left and right
columns is the same as that corresponding to Figures 3 and 4, and that in
the middle column is intermediate between them. There is clearly an important
effect of the image vortex within the leading-edge on the distortion and
trajectory of the incident primary vortex. The question arises as to whether
it is possible to simulate this effect using a simple point vortex, where a
very thin leading-edge would be simulated simply by a thin plate, and the
thick elliptical leading-edge by an elliptical section. In doing so, it
would be possible to physically explain why the larger scale of the leading-
edge causes the incident primary vortex to dive beneath the edge, instead
of being severed at its tip.

The interaction mechanism corresponding to the case where the incident
vortex is above the leading-edge is shown in Figures 7 and 8, for hydrogen
bubble wires well upstream of and at the tip of the leading edge respectively.
In this case, there is no evidence of secondary vortex formation. Rather,
there tends to be a "lifting up" of the primary vortex as it negotiates
the upper surface of the edge. Pressure measurements will provide detailed
insight into the importance of this type of vortex interaction and distortion
in inducing the pressure field, relative to the case where the vortex dives
beneath the leading-edge.

2

A sample of the instantaneous pressure distribution for the case where the incident vortex dives beneath the edge is given in Figure 9. To the left of each photo is the instantaneous pressure distribution (indicated by the dark-shaded area) as well as the time-averaged pressure amplitude (indicated by the vertical lines). We note, at this point, that, of course, the pressure amplitude is to be measured normal to the local surface tangent; this point may be of confusion if one views the vertical solid lines. These pressure distributions show, first of all, that the maximum pressure amplitude does not appear at the tip of the edge, but rather downstream of it. The maximum-negative pressure pocket tends to follow the primary-secondary vortex pair as it travels down beneath the surface of the edge. Moreover, the pressure distribution indicates a wave-like form due to the finite wavelength between successive vortices. However, we feel that the wavelength between vortices is sufficiently large that one may consider the interaction process to be basically that of a single vortex impinging upon the edge. Note that along the upper surface of the leading-edge, there are minor streamwise phase variations of the instantaneous pressure field except in the region very near the tip. This is due to the fact that the incident vorticity wave travels primarily beneath, rather than above, the tip of the edge. The pressure fluctuations on the upper surface are characteristically smaller amplitude, and due to the potential field distortion there, arising from passage of the primary vortex beneath the edge.

Figure 10 shows instantaneous and time-averaged pressure contours excerpted from Figure 9 with three different types of flow visualization, all taken at the same instant during the interaction process. All visualization sequences show clearly the process of secondary vortex formation of the other side of the edge. In the coming months, it is planned to complete a series of these photos in order to provide a composite view of the effect of vortex distortion and trajectory on instantaneous pressures visualized using the three different hydrogen bubble wire techniques.

A central part of our investigation is to determine the effect of scale of the incident vortex relative to that of the leading-edge. Figures 11, 12 and 13 show preliminary, exploratory studies of the effect of a vortex street interacting with a relatively thick leading-edge. We are still in

3

the process of characterizing the circulation and length scale of the
incident vortices in the street. However, these initial studies do
indeed show some interesting features not evident in the previous cases.
In Figure 11, the vortex street impinges symmetrically upon the leading-
edge, and there is severe distortion of the vortices passing along the
upper and lower surfaces. Accompanying this distortion is a substantial
increase in the wavelength between vortices (upper left photo). The
remaining photos show visualization for the case where the hydrogen bubble
wire was located at the tip of the edge, with varying pulse frequencies
and widths. There is clearly a wavelike motion due to the distorted incident
vortex travelling along the upper surface. However, there is no evidence
of secondary vortex formation. In Figure 12, we consider the case where
the incident vortex street passes along the upper surface of the leading-
edge. In this case, the incident vortex street retains, in a remarkably
coherent fashion, its identity, though there tends to be rearrangement of
the incident vortex array towards a single row of vortices of alternating
sense as the street is swept along the surface of the edge. The refined
visualization shown with the wire located at the tip of the edge evidences
the fact that there is no secondary vortex formation. In essence, this
is due to the fact that the circulation of each of the vortices is considerably
smaller than those for the previous case of single vortex edge interaction;
moreover, there is certainly a mutual induction effect between alternating
vortices of opposite sense that may well preclude secondary vortex formation.
In Figure 13, the incident vortex street is located still further above
the surface of the leading-edge. Again, there is no evidence of secondary
vortex formation, and the incident vortex street retains its coherence
remarkably well. It is proposed to extend this investigation to examine
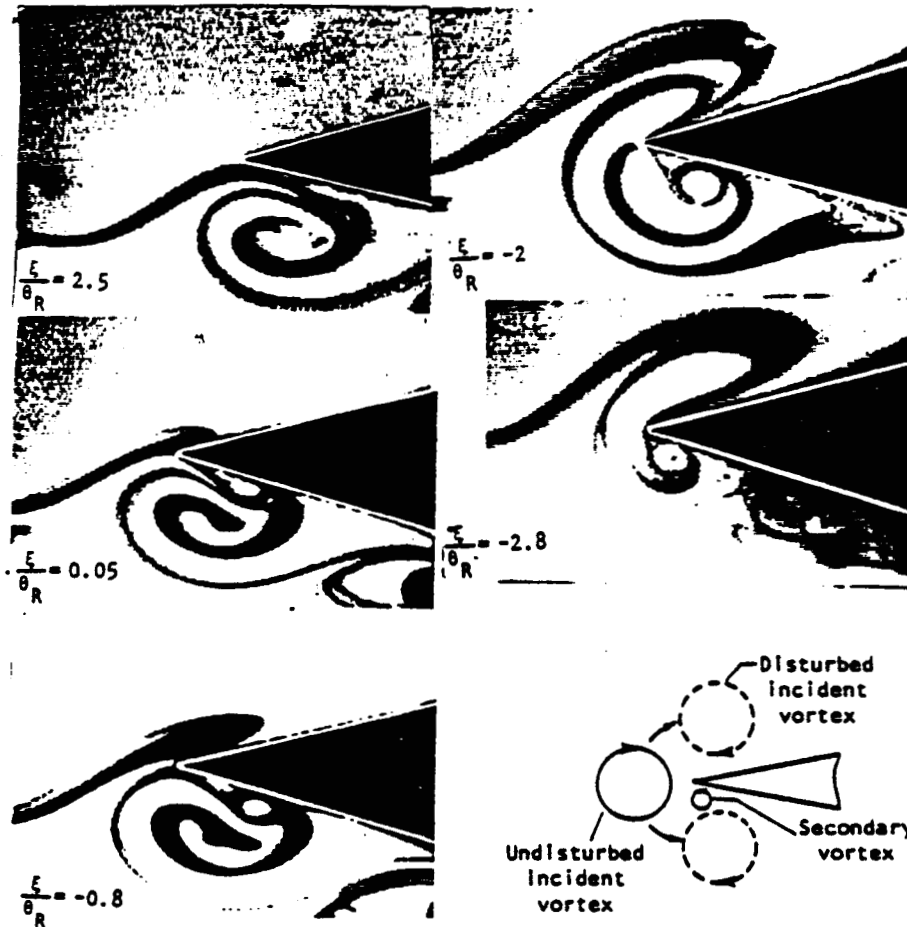the effect of vortex scale, circulation, and wavelength on the induced
pressure field.

Figure 1: The type of interaction mechanism and extent of secondary vortex shedding strongly depends upon location of incident vortex with respect to leading-edge.
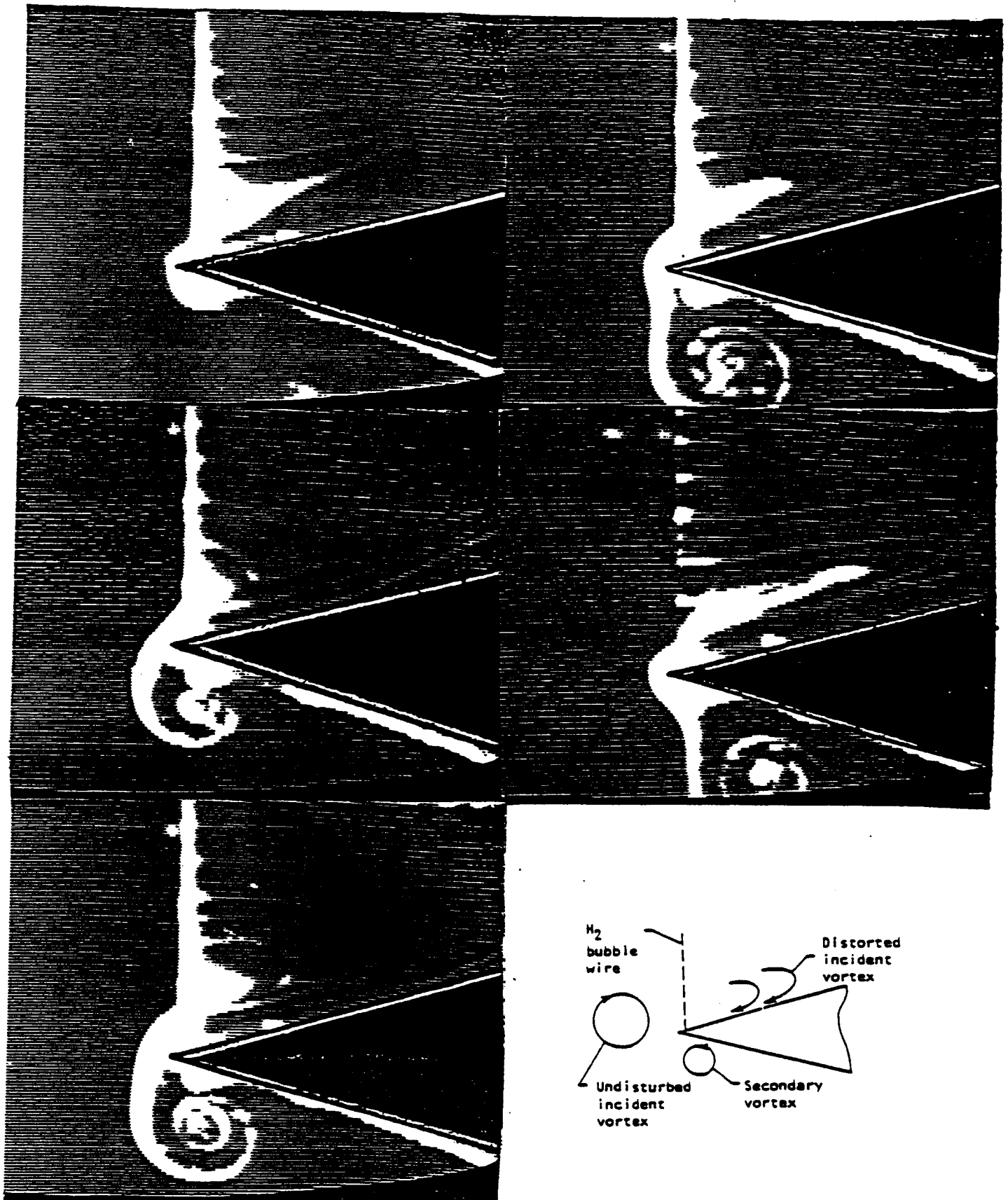
Figure 2: Streaklines generated from hydrogen bubble wire show sweeping of flow chart tip of edge during formation of secondary vortex.

Figure 3: Effect of edge thickness on the interaction; vortex incident upon a 5:1 elliptical leading-edge. $(2T/\Delta\omega = 0.7; 2T/\theta_R = 3.3)$

7

Figure 4: Vortex interaction with 5:1 elliptical leading-edge; block
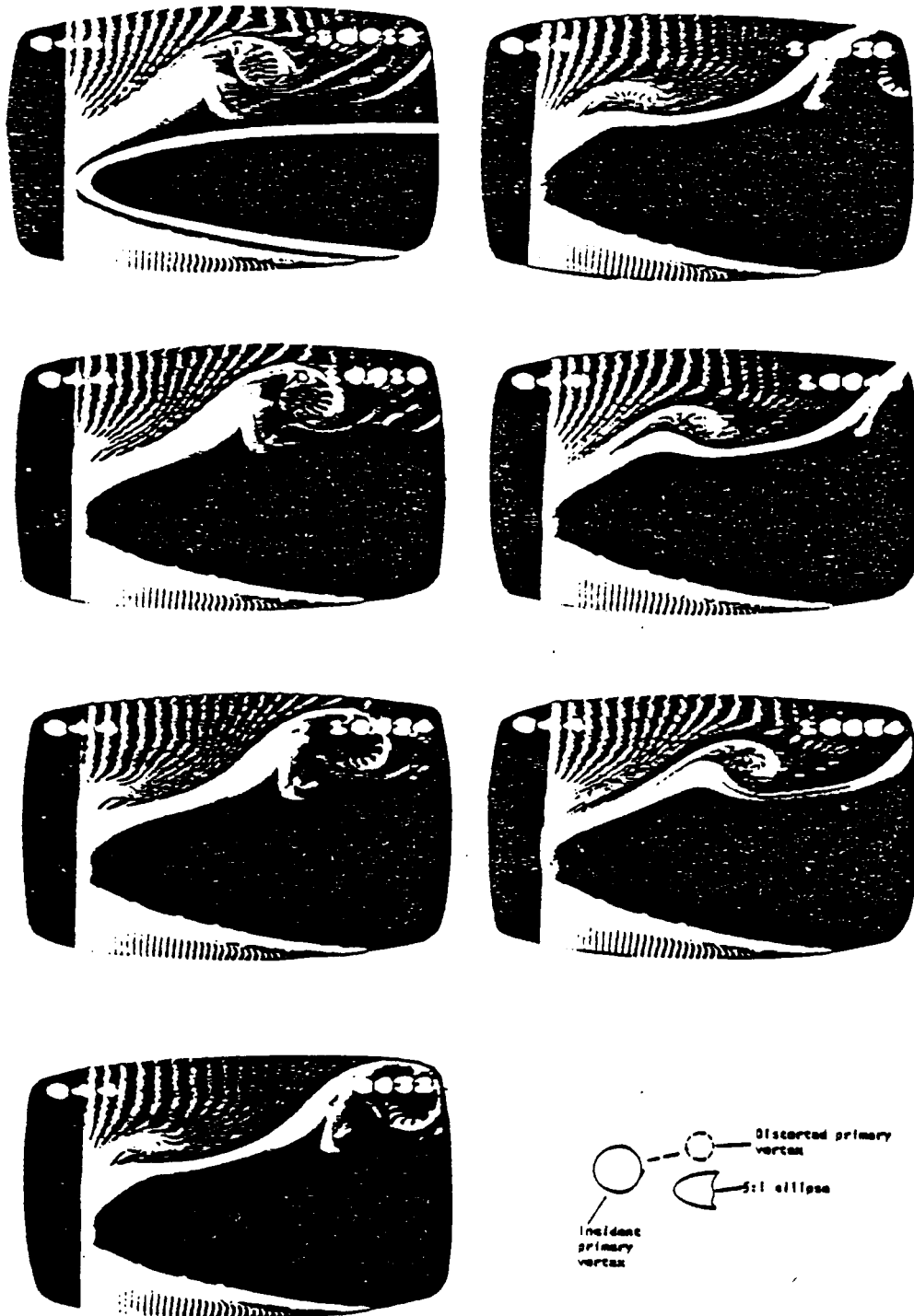of hydrogen bubble lines generated upstream of the leading-
edge ($\xi/2T=0$).
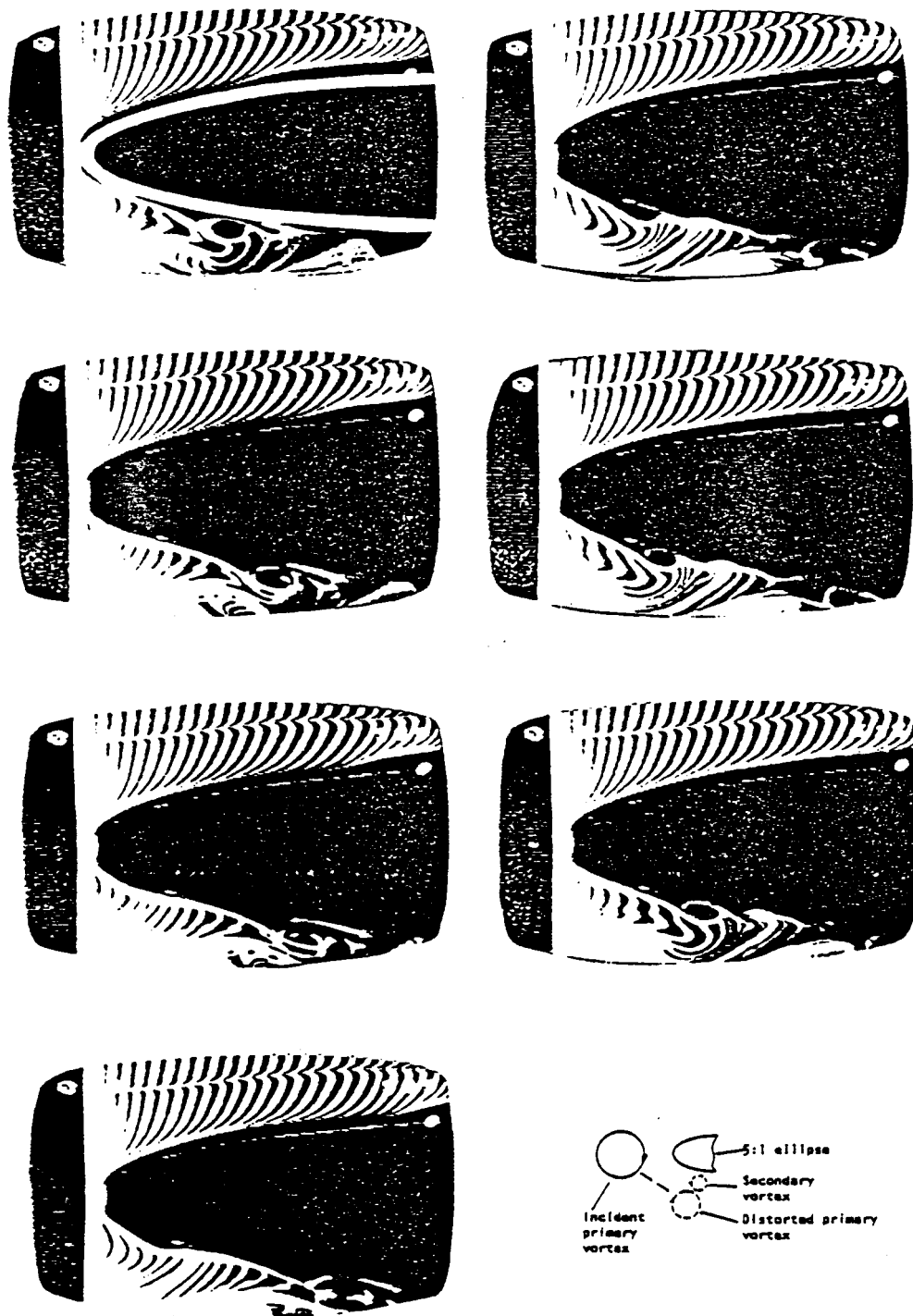
Figure 5:   Vortex interaction with 5:1 elliptical leading-edge;
finely pulsed hydrogen bubble lines generated at the top
of the leading-edge ($\xi/2T=0$).

9
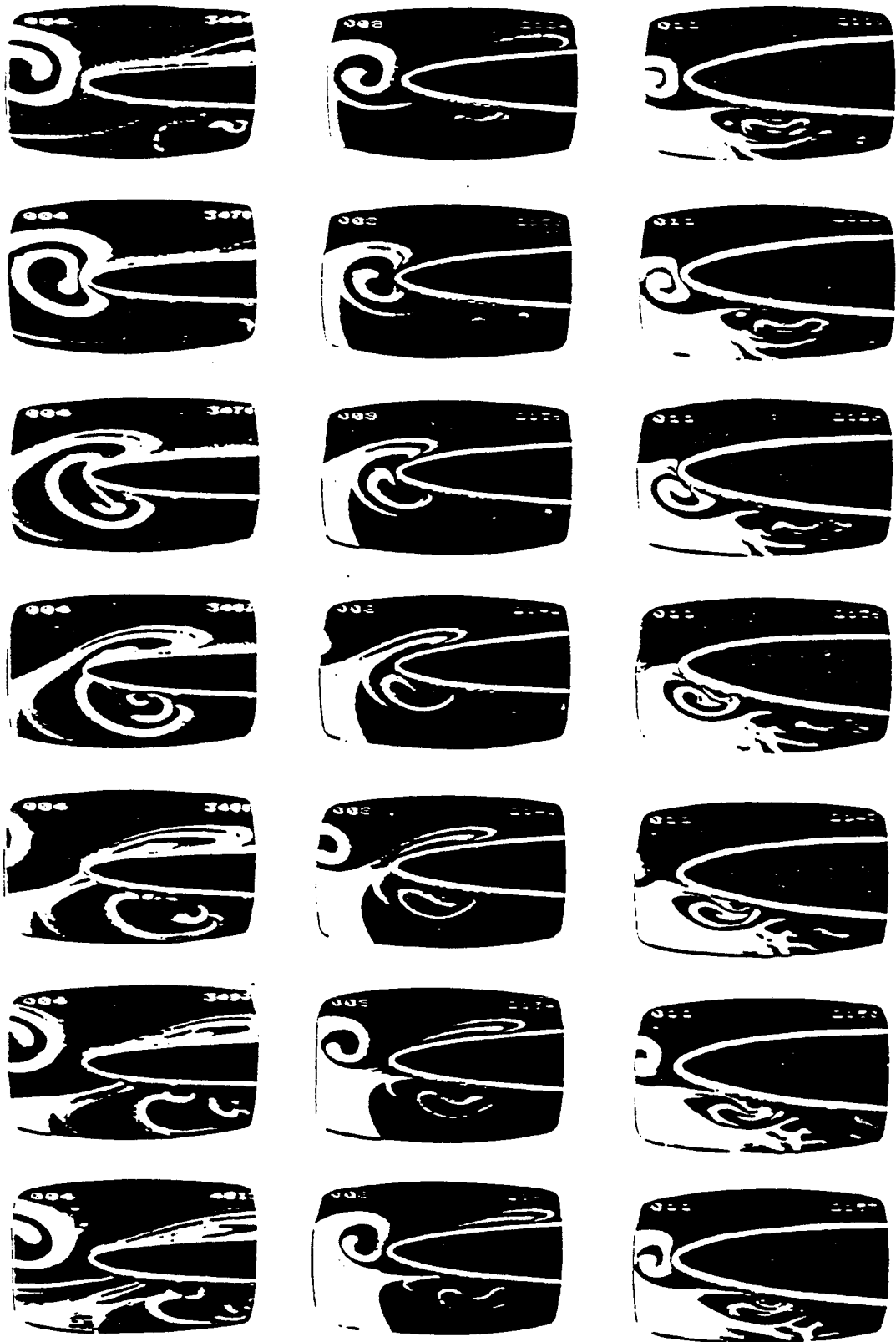
Figure 6: Effect of edge thickness on the interaction; comparison of different thickness 5:1 elliptical leading-edges.

10
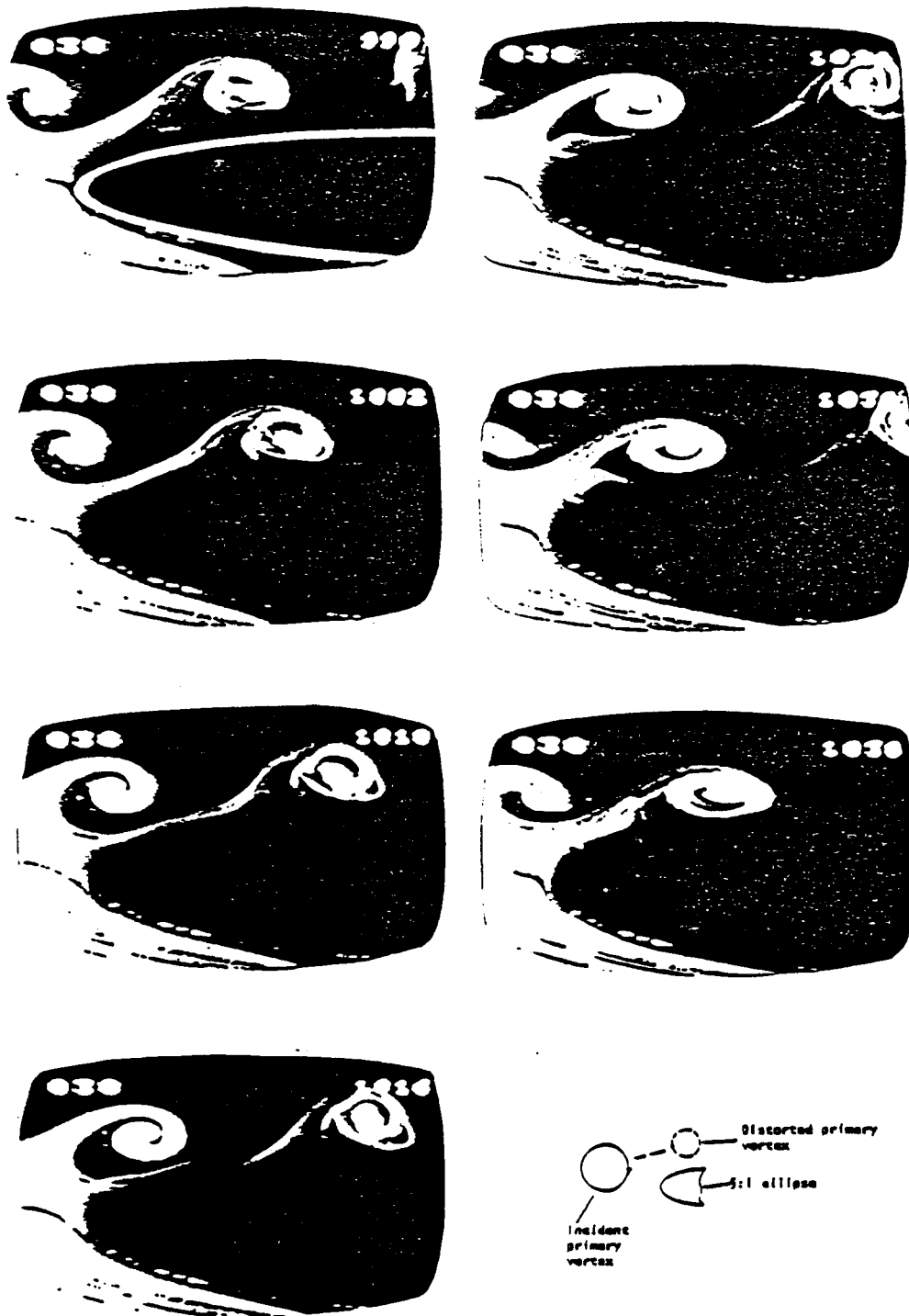
Figure 7: Vortex interaction with 5:1 elliptical leading-edge;
block of hydrogen bubble lines generated upstream of
the leading-edge ($\xi/2T=-0.4$).

11

Figure 8:   Vortex interaction with 5:1 elliptical leading-edge;
finely pulsed hydrogen bubble lines generated at the tip
of the leading-edge ($\xi/2T=-0.4$).
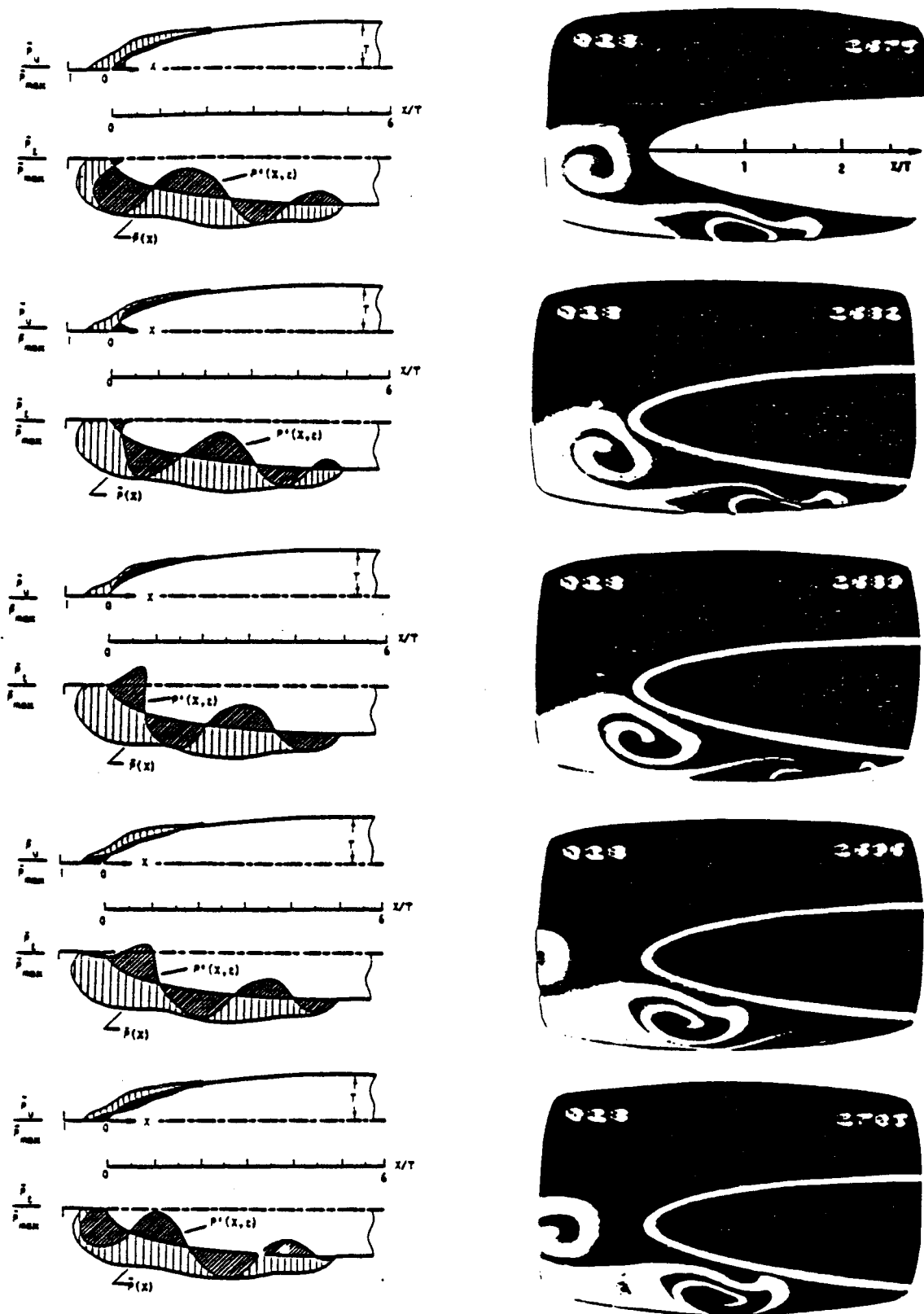
Figure 9:   Instantaneous pressure fields and corresponding vortex-
            edge interaction mechanisms for various locations of vor-
            tex relative to leading-edge; i.e. for different times
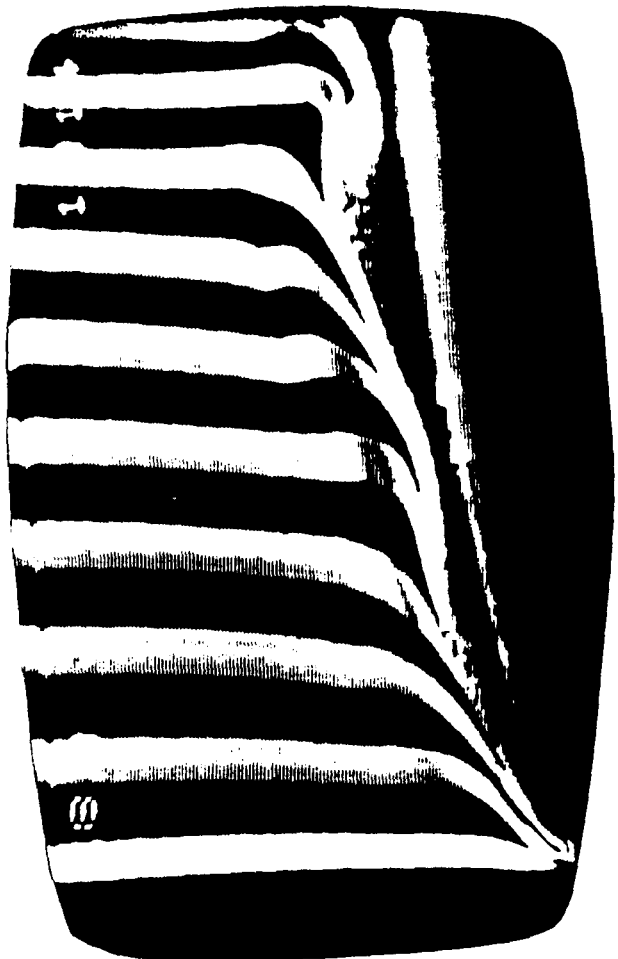   (t=0, 1/5 T, 2/5 T, 3/5 T, 4/5 T; ξ/2T=0.1).
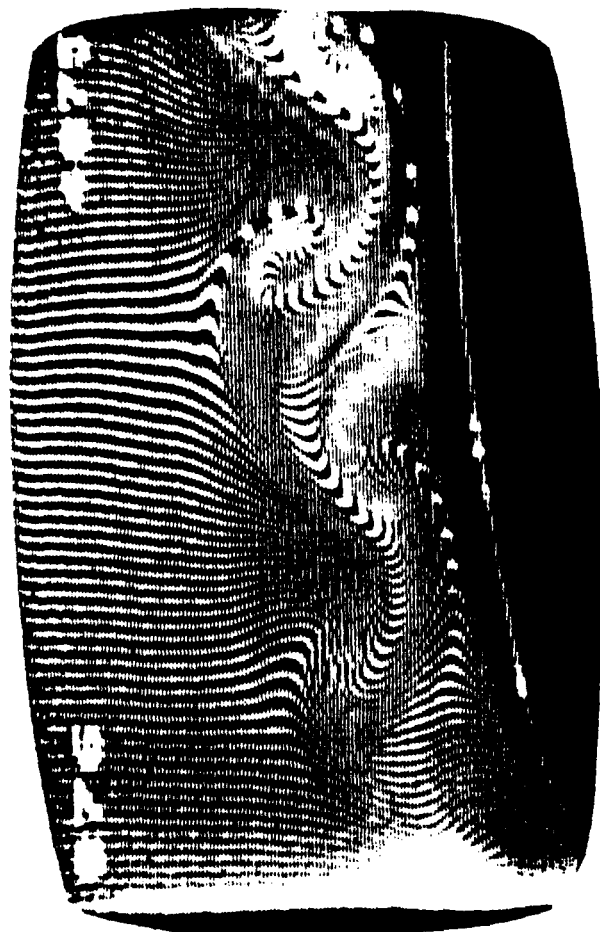
13
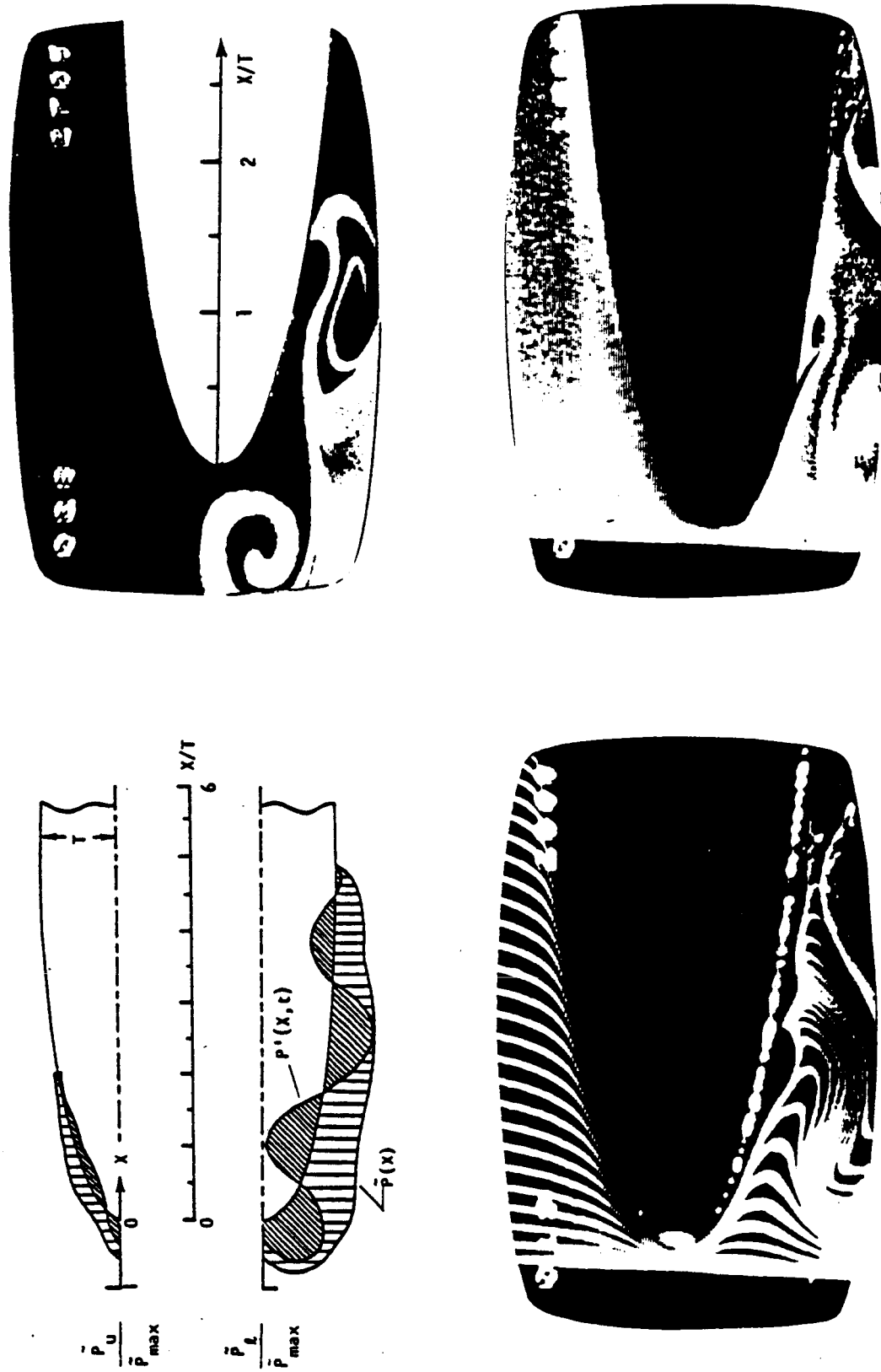
Figure 10: Instantaneous pressure fields and three different visualizations of corresponding flow field at t=4T/5 ($\xi/2T=0.1$).
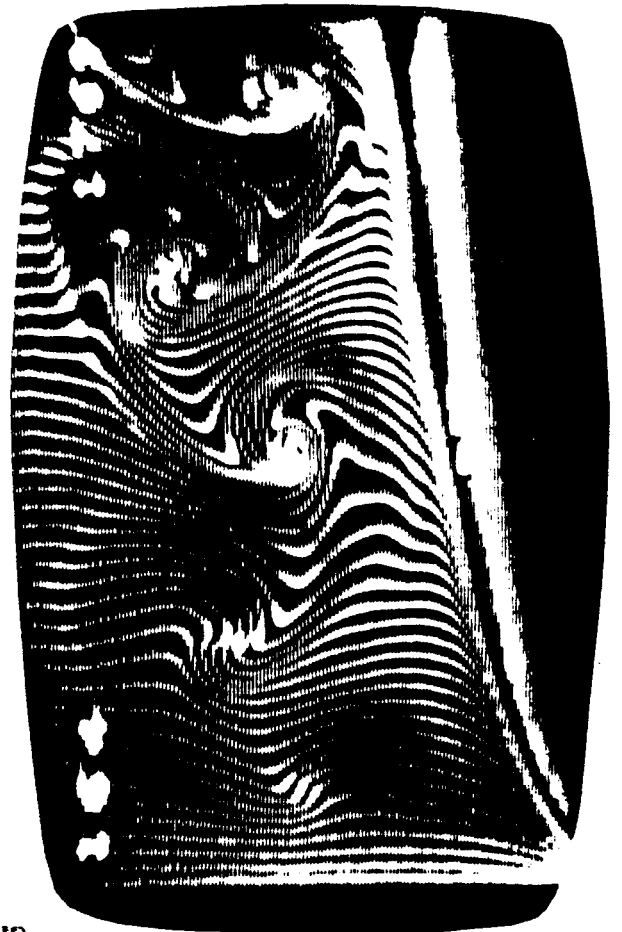
14

17